

# High-precision measurement of the atomic mass of $^{84}\text{Sr}$ and implications to isotope shift studies

Z. Ge,<sup>1,\*</sup> S. W. Bai,<sup>2</sup> T. Eronen,<sup>1</sup> A. Jokinen,<sup>1</sup> A. Kankainen,<sup>1</sup> S. Kujanpää,<sup>1</sup> I. D. Moore,<sup>1</sup> D. A. Nesterenko,<sup>1</sup> and M. Reponen<sup>1</sup>

<sup>1</sup>*University of Jyväskylä, Department of Physics, Accelerator laboratory, P.O. Box 35, FI-40014, Jyväskylä, Finland*

<sup>2</sup>*School of Physics and State Key Laboratory of Nuclear Physics and Technology, Peking University, Beijing 100871, China*

(Dated: April 3, 2024)

The absolute mass of  $^{84}\text{Sr}$  was determined using the phase-imaging ion-cyclotron-resonance technique with the JYFLTRAP double Penning trap mass spectrometer. A more precise value for the mass of  $^{84}\text{Sr}$  is essential for providing potential indications of physics beyond the Standard Model through high-precision isotope shift measurements of Sr atomic transition frequencies. The mass excess of  $^{84}\text{Sr}$  was refined to be  $-80649.229(37)$  keV/c<sup>2</sup> from high-precision cyclotron-frequency-ratio measurements with a relative precision of  $4.8 \times 10^{-10}$ . The obtained mass-excess value is in agreement with the adopted value in the Atomic Mass Evaluation 2020, but is 30 times more precise. With this new value, we confirm the previously observed nonlinearity in the study of the isotope shift of strontium. Moreover, the double-beta ( $2\beta^+$ ) decay  $Q$  value of  $^{84}\text{Sr}$  was directly determined to be  $1790.115(37)$  keV, and the precision was improved by a factor of 30.

## I. INTRODUCTION

Isotope shifts in atomic transition frequencies arise from differences in neutron numbers among isotopes sharing the same atomic number. The isotopic shifts in the frequency of an atomic transition demonstrate an approximately linear correlation with the isotope shift observed in a second transition. These shifts reveal contributions from field and mass shifts [1], originating from the differing nuclear masses of isotopes and variations in their nuclear charge distribution. Isotopic shifts can be systematically studied using a King plot analysis. In this analysis, the isotope shifts in two sets of electronic transitions within the same isotopes are correlated. To perform the King plot analysis, one measures the energies of two transitions for three or more isotopes of a specific element. The King plot is expected to exhibit linearity, with the experimentally determined slope serving as a reliable benchmark for theoretical predictions [2]. Deviations from linearity are crucial for refining atomic structure calculations [3–5]. Recent theoretical proposals suggest that the linearity in King plots could be leveraged to impose constraints on higher-order effects on isotope shifts or on physics beyond the Standard Model (SM) [6, 7]. Motivated by this, a recent surge in efforts [8–19] has significantly advanced the precision of isotope shift measurements. Essential to placing constraints on proposed electron-neutron interactions and other novel physics through King’s linearity is a two-fold requirement. First, experimental data in the form of precision optical spectroscopy and nuclear mass measurements are needed to empirically limit the potential size of the nonlinearity. Second, if a nonlinearity is observed, precise atomic and nuclear theory is necessary to calculate beyond-first-order SM sources of nonlinearity. A natural inquiry emerges regarding the potential for the King plot to maintain its linearity at an enhanced level of experimental precision. Recent experiments conducted with strontium and ytterbium ions [8, 14] have provided initial indications that this linearity is, in fact, disrupted at a magnitude of several standard deviations.

Strontium presents favorable properties for studying isotope shifts, boasting an abundance of stable isotopes and very narrow optical transitions [20]. Earlier theoretical work has also proposed the measurement of strontium isotope shifts as a promising probe for new physics [6, 7]. Strontium features four stable isotopes: three bosons ( $^{84,86,88}\text{Sr}$ ) and one fermion ( $^{87}\text{Sr}$ ). Precise and accurate determination of the atomic mass of the stable Sr isotopes is crucial for probing potential causes for such nonlinearities.

Atomic masses of  $^{86-88}\text{Sr}$  have been measured at the FSU Penning trap [21] with high precision (uncertainty of  $\leq 6$  eV/c<sup>2</sup>) as adopted in the most recent Atomic Mass Evaluation 2020 (AME2020) [22, 23]. The atomic mass uncertainty for  $^{84}\text{Sr}$ , the least abundant naturally occurring isotope of strontium, is however notably higher at 1.2 keV/c<sup>2</sup>. For investigating fundamental physics and exploring phenomena beyond the SM via high-precision King-plot tests with strontium, it is critical to measure the atomic mass of  $^{84}\text{Sr}$  directly with high precision. In this article, we report on the most precise absolute mass value of  $^{84}\text{Sr}$  to date, achieved via high-precision cyclotron-frequency-ratio measurements with the JYFLTRAP double Penning trap mass spectrometer (PTMS). We employ this refined mass value in an updated King plot analysis for two transitions of strontium.

## II. EXPERIMENTAL METHOD

The experiment was performed at the Ion Guide Isotope Separator On-Line facility (IGISOL) using the JYFLTRAP double PTMS [24, 25], at the University of Jyväskylä [26]. Stable  $^{84}\text{Sr}^+$  ions were generated using an offline glow-discharge ion source. For a precise mass measurement of  $^{84}\text{Sr}$ , reference ions of  $^{84}\text{Kr}^+$  with a well-known mass value (uncertainty of 4 eV/c<sup>2</sup> [22]) were concurrently produced from the same ion source. As illustrated in Fig. 1(a), the gas cell within the glow-discharge ion source comprises two sharp electrodes, with one composed of naturally abundant strontium. By introducing a gas containing natural krypton, it facilitates the simultaneous generation of stable ions for both strontium and krypton.

\* Corresponding author: zhuang.z.ge@jyu.fi

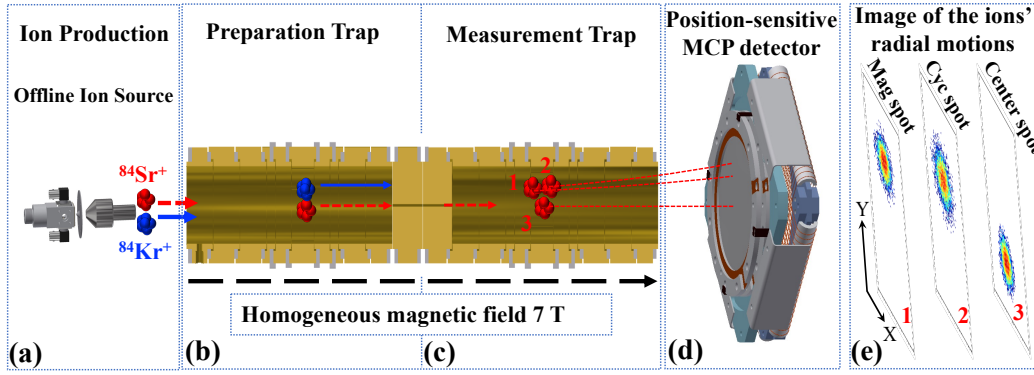


FIG. 1. (Color online). (a) Diagram depicting the ion production and mass measurement process using the PI-ICR technique. Stable  $^{84}\text{Sr}^+$  and  $^{84}\text{Kr}^+$  ions were concurrently generated in an offline glow-discharge ion source. Selection of the final ion species occurred through buffer-gas cooling in the preparation trap (b), and the cyclotron frequency was determined using the phase-imaging technique at the measurement trap (c). (d) The position-sensitive MCP detector captured the projected images representing different radial-motion phases (1-3). (e) Illustration depicting the radial-motion (1: "magnetron", 2: "cyclotron", and 3: "center") projection of  $^{84}\text{Sr}^+$  ions onto the position-sensitive MCP detector. Panel 1 shows the magnetron phase spot, panel 2 the cyclotron phase spot, and panel 3 the center spot. The angle difference between magnetron and cyclotron motion spots relative to the center spot was used to deduce the cyclotron frequency of the measured ion. Colors in each pixel indicate the number of ions.

The generated ions of  $^{84}\text{Sr}^+$  and  $^{84}\text{Kr}^+$  were extracted using helium gas flow and electric fields facilitated by a sextupole ion guide (SPIG) [27]. Following acceleration over an electric potential of  $\approx 30$  kV, the ions with mass number of  $A = 84$  were mass-separated using a  $55^\circ$  dipole magnet with a mass resolving power of  $M/\Delta M \approx 500$ . Post isobaric separation, the ions were directed to a radiofrequency quadrupole cooler-buncher (RFQ) [28], where they were accumulated, cooled, and bunched.

The ion bunches from the RFQ were injected to the JYFLTRAP double PTMS, consisting of two cylindrical Penning traps equipped with a 7-T superconducting solenoid. The first trap, functioning as a purification trap, is filled with buffer gas and is employed for isobaric purification using the side-band buffer gas cooling technique [29]. This technique alone achieves mass purification with a resolving power of approximately  $10^5$  by selectively converting ion motion from magnetron to reduced cyclotron motion.

In the purification trap, all cooled and centered ions ( $^{84}\text{Sr}^+$  and  $^{84}\text{Kr}^+$ ) were initially excited to a large orbit of revolution by applying a dipole excitation at the magnetron motion frequency  $\nu_-$  for approximately 11 ms. Subsequently, a quadrupole excitation was executed to center the ions of interest (only  $^{84}\text{Sr}^+$  or  $^{84}\text{Kr}^+$ ) through collisions with the buffer gas for about 100 ms.

In the precision trap, the phase-imaging ion-cyclotron-resonance (PI-ICR) method [30, 31] was employed to measure the actual cyclotron frequency,  $\nu_c = qB/(2\pi m)$ , where  $B$  is the magnetic field strength,  $q$  is the charge state, and  $m$  is the mass of the stored ion. The scheme of the PI-ICR technique [30–33] at JYFLTRAP relies on direct measurements of the cyclotron motion and magnetron motion simultaneously by projecting their radial ion motion onto a position-sensitive MCP detector.

To determine the phases of the radial motions, the center has to be determined for the ion spots on the detector. This is

done by storing the ions for a few milliseconds without exciting their cyclotron motion, and the ions are directly extracted from the trap and projected onto the MCP detector.

Two patterns, as detailed in [30, 31], are utilized to measure the magnetron or cyclotron motion phases, respectively. The angle between two phase images of the projected radial motions with respect to the center spot is  $\alpha_c = \alpha_+ - \alpha_-$ , where  $\alpha_+$  and  $\alpha_-$  are the polar angles of the cyclotron and magnetron motion phases. The cyclotron frequency  $\nu_c$  is derived from:

$$\nu_c = \frac{\alpha_c + 2\pi n_c}{2\pi t_{acc}}, \quad (1)$$

where  $n_c$  is the full number of revolutions of the measured ions during the phase accumulation time  $t_{acc}$ . A few different accumulation times for  $^{84}\text{Sr}^+$  and  $^{84}\text{Kr}^+$  were used to confirm the unambiguity of the cyclotron frequency. A fixed accumulation time of 400 ms was employed for the actual measurements to determine the final  $\nu_c$ . A measurement with "cyclotron" and "magnetron" phase spots collected with respect to the center spot is shown in Fig.1(b).

The atomic mass  $M_{^{84}\text{Sr}}$  was derived from the measured cyclotron frequency ratio ( $R = \nu_c(^{84}\text{Kr}^+)/\nu_c(^{84}\text{Sr}^+)$ ) measurements of singly charged ions of the decay pair  $^{84}\text{Sr}-^{84}\text{Kr}$ :

$$M(^{84}\text{Sr}) = R(M(^{84}\text{Kr}) - qm_e) + qm_e + (R \cdot B(^{84}\text{Kr}) - B(^{84}\text{Sr}))/c^2, \quad (2)$$

Here,  $M(^{84}\text{Sr})$  and  $M(^{84}\text{Kr})$  represent the respective masses of the parent and daughter atoms, and  $q$  denotes the charge state for singly charged ions ( $q = 1$ ).  $m_e$  and  $c$  correspond to the mass of an electron and the speed of light in vacuum. The electron binding energies,  $B(^{84}\text{Sr})$  and  $B(^{84}\text{Kr})$ , are 5.69486745(12) eV and 13.9996055(20) eV, respectively, as obtained from [34].

The  $Q$  value for the double-beta decay of  $^{84}\text{Sr}$  can be determined from the mass difference:  $Q_{2\beta^+} = (M(^{84}\text{Sr}) -$

$$M(^{84}\text{Kr}))c^2.$$

TABLE I. The resulting  $Q_{2\beta^+}$  and mass-excess values of  $^{84}\text{Sr}$  determined in this work based on the weighted mean of the cyclotron frequency ratio  $\bar{R}$ . The frequency ratio  $\bar{R}$ ,  $Q_{2\beta^+}$  values (in keV), and the mass excess (ME, in keV/c<sup>2</sup>) of the parent, as determined in this work, are provided alongside the corresponding values from AME2020 [22] for comparison.

	$\bar{R}$	$Q_{2\beta^+}$	ME
This Work	1.000 022 902 36(48)	1790.115(37)	-80649.229(37)
AME2020		1789.8(12)	-80649.6(12)

### III. RESULTS AND DISCUSSION

#### A. Mass and $Q$ -value determination

A full scanning measurement (one cycle) of the magnetron phase, cyclotron phase, and center spot in sequence was completed in less than 3 minutes for each ion species of  $^{84}\text{Kr}^+$  and  $^{84}\text{Sr}^+$ . In the analysis, the position of each spot was fit using the maximum likelihood method. A few cycles were summed to ensure reasonable counts for fitting before determining the position of each spot. The phase angles were calculated accordingly based on the determined positions of the phases to deduce the cyclotron frequencies of each ion species. The cyclotron frequency  $\nu_c$  of the daughter ion  $^{84}\text{Kr}^+$  was used as a reference and was linearly interpolated to the time of the measurement of the parent  $^{84}\text{Sr}^+$  (ion of interest) to deduce the cyclotron frequency ratio  $R$ . Bunches with less than five detected ions per bunch were considered in the data analysis to reduce a possible cyclotron frequency shift due to ion-ion interactions [35, 36]. Up to 5 detected ions per bunch were taken into account for the analysis, and no count-rate related frequency shifts were observed in the analysis. The temporal fluctuation of the magnetic field for JYFLTRAP was measured to be  $\delta_B(\nu_c)/\nu_c = \Delta t \times 2.01(25) \times 10^{-12}/\text{min}$  [31], where  $\Delta t$  is the time interval between two consecutive reference measurements. The contribution of temporal fluctuations of the magnetic field to the final frequency ratio uncertainty was less than  $10^{-10}$  since the parent-daughter measurements were interleaved with  $\Delta t < 10$  minutes. To minimize the systematic uncertainty arising from the conversion of cyclotron motion to magnetron motion and potential distortion of the ion-motion projection onto the detector, the positions of the magnetron-motion and cyclotron-motion phase spots were deliberately chosen. The angle  $\alpha_c$  between them was kept to a few degrees or less, effectively reducing this uncertainty to a level well below  $10^{-10}$  [32]. Moreover, the commencement of the initial dipolar excitation with frequency  $\nu_+$  was systematically scanned across one magnetron period (6 points), and the extraction was scanned over one cyclotron period (6 points) to mitigate any lingering effects of residual magnetron and cyclotron motion that might influence the distinct spots. The measurements were conducted in eight separate time slots,

each lasting around 4 hours. For each slot of measurement, a weighted mean ratio  $R_{4h}$  was calculated, and the maximum of internal and external errors [37] was selected. The final ratio  $\bar{R}$  was then obtained as a weighted mean ratio of all  $R_{4h}$  sets, taking into account the maximum of internal and external errors. The systematic uncertainties and experimental statistical uncertainty were added in quadrature to the final result. The final frequency ratio  $\bar{R}$  with its uncertainty, as well as the corresponding  $Q_{2\beta^+}$  and mass-excess values, are 1.000 022 902 36(48), 1790.115(37) keV, and -80649.229(37) keV/c<sup>2</sup> respectively.

In Fig. 2, the analysis results, which include all data sets, are compared to literature values. A comparison of these results to the literature values are also tabulated in Table. I.

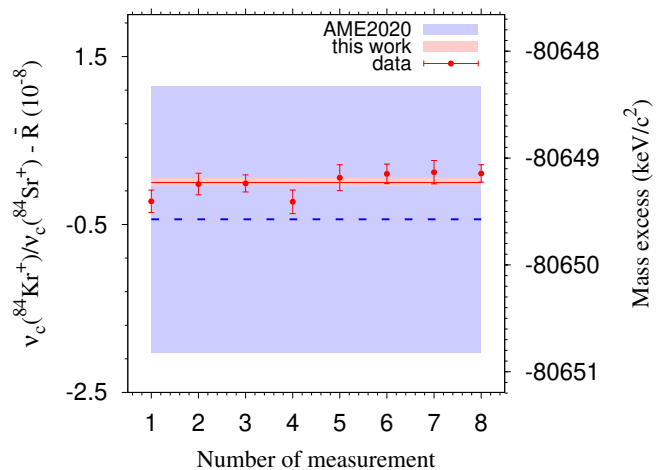


FIG. 2. (Color online). The deviation (left axis) of the individually measured cyclotron frequency ratios  $R_{4h}$  ( $\nu_c(^{84}\text{Kr}^+)/\nu_c(^{84}\text{Sr}^+)$ ) from the final ratio value  $\bar{R}$  and (right axis) mass-excess values in this work compared to values adopted from AME2020 [22, 38]. The red points, accompanied by uncertainties, represent individual data obtained with the PI-ICR method in eight distinct time slots. The solid red line illustrates the weighted average value from this work,  $\bar{R} = 1.000\ 022\ 902\ 36(48)$ , and its  $1\sigma$  uncertainty band is shaded in red. The dashed blue line represents the difference between the new value in this work and the one referred to in AME2020, with its  $1\sigma$  uncertainty area shaded in blue.

The mass excess (-80649.229(37) keV/c<sup>2</sup>) and  $Q_{2\beta^+}$  (1789.8(12) keV) from this work are both a factor of  $\approx 30$  more precise than those derived from the evaluated masses in AME2020 [22, 38], but both agree well with the values documented in AME2020. The mass-excess value in AME2020 is derived primarily from two PTMS experiments [39, 40] with an influence of 88.8%. A slight contribution of 6.8% is from endpoint energy measurements of  $^{84}\text{Rb}(\beta^-)^{84}\text{Sr}$  [41] and the smallest influence of 2.1% is related to a nuclear reaction experiment  $^{84}\text{Sr}(d,p)^{85}\text{Sr}$  [42].

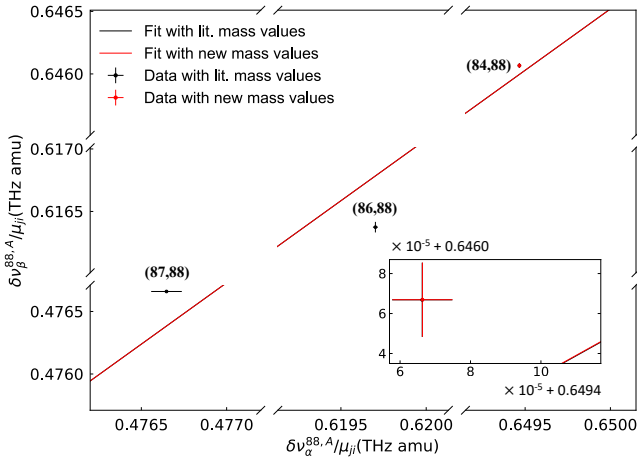


FIG. 3. (Color online). King plot of the strontium isotope shifts in  $\alpha$  (689 nm) and  $\beta$  (698 nm) transitions as reported in [8, 43]. The implication of the mass value of  $^{84}\text{Sr}$  from this work compared to values adopted from AME2020 [22, 38] is evident. Black data points and their accompanying error bars in black are obtained using the literature mass values, while the red data point with error bars is obtained with the new mass value from this work. Error bars and the difference between the  $^{84}\text{Sr}$ - $^{88}\text{Sr}$  points derived from our measurement and from [8, 22, 38, 43] are not visible at the scale being used due to a good agreement of this work with the AME2020. Linear fits were conducted for the set with literature data (black) and the new mass value (red), with a zoomed-in inset demonstrating a rather small change in the linear fit and no significant change in nonlinearity.

## B. King plot analysis

The isotope shift between two isotopes with mass numbers  $A_1$  and  $A_2$ , ( $v_i^{A_1 A_2}$ ) is defined as the difference in transition frequencies:  $v_i^{A_1 A_2} = v_i^{A_1} - v_i^{A_2}$ . The primary contributions to the isotope shift arise from the mass shift (MS) and field shift (FS). The MS results from the mass difference of isotopes  $A_1$  and  $A_2$  and is expressed as an electronic coefficient  $k_i$  multiplied by the isotope-dependent reduced mass, given by:  $\mu_{A_1 A_2} = 1/m_{A_1} - 1/m_{A_2}$ . The FS originates from the differing volumes of the two isotopes, factorized into an electronic, isotope-independent coefficient  $F_i$  and the charge radius variance  $\delta\langle r^2 \rangle_{A_1 A_2} = \langle r_{A_1}^2 \rangle - \langle r_{A_2}^2 \rangle$ . The isotope shift composition in terms of electronic and nuclear quantities factorizes into the total isotope shift equation:  $v_i^{A_1 A_2} = k_i \mu_{A_1 A_2} + F_i \delta\langle r^2 \rangle_{A_1 A_2} + \dots$ , where the first term represents the MS, and the second term represents the FS [1, 44], with the dots denoting potential higher-order corrections and new physics contributions. The frequency shifts are commonly normalized by the reduced mass  $\mu_{A_1 A_2}$  to obtain the modified isotope shift,  $v_i^{A_1 A_2} / \mu_{A_1 A_2}$ . Consequently, the MS (the sum of the normal MS and specific MS) reduces to the electronic factor  $k_i$ , while the FS factor  $F_i$  is multiplied by the modified charge radius variance,  $\delta\langle r^2 \rangle_{A_1 A_2} / \mu_{A_1 A_2}$ , establishing a linear dependence between the two sets of modified frequency shifts known as the King linearity [44]. To quan-

tify the observed linearity, a measure of nonlinearity is defined [2, 45]. A King plot analysis can be used to systematically quantify and visually examine isotope shifts in various atomic transitions referenced to the same isotope.

The refined mass-excess value obtained for  $^{84}\text{Sr}$  was employed to carry out an updated King plot analysis for two transitions at 589 nm and 598 nm, as detailed in [8, 43]. Figure 3 displays the King plot featuring both the literature mass values from AME2020 and our updated mass value. The main uncertainties in the plot are from the frequency shifts measurements in the transitions between  $^{84}\text{Sr}$ ,  $^{86}\text{Sr}$ , and  $^{87}\text{Sr}$  relative to  $^{88}\text{Sr}$  as adopted from [8]. The transition of  $^{84}\text{Sr}$ - $^{88}\text{Sr}$  at 598 nm is from [43] which has a better precision than that of [8]. The observed nonlinearity from [8], achieved through our new mass value for  $^{84}\text{Sr}$  is evident, and the uncertainty is no longer constrained by the mass uncertainty. Given that the uncertainty in the mass contributes to the calculation of the modified isotope shifts in similar ways, the impact on the linearity of the King plot is preserved due to the agreement of our result with the literature value.

A linear orthogonal distance regression analysis [46] that provides unified standard error estimates for the uncertainties implanted in  $x$  and  $y$  directions, was conducted to determine the slope and intercept. The resulting slope and intercept from the fit to the AME2020 mass values and the updated mass value are 0.98148(51) and 8578(326) MHz $\cdot$ amu, respectively. Our results align well with the fitting values of 0.981(5) and 8560(3450) MHz $\cdot$ amu, reported in [8], offering smaller uncertainties. These results confirm the nonlinearity announced in [8], using the nonlinearity measure defined in [2, 45]. The uncertainty from the mass values now allows for a potential future precision measurement of optical spectroscopy to reach a relative precision by more than three orders of magnitude, thus potentially leading to an unprecedented sensitivity for new physics. This will reach the spectroscopic precision necessary to attain state-of-the-art bounds on a spin-independent fifth force, as current calculations place the required uncertainty at  $< 1$  Hz [45, 47]. This would essentially demand measuring optical atomic transitions with a relative precision of  $10^{-15}$  or lower, a challenging accomplishment feasible only for a select few leading optical clock laboratories [47].

## IV. CONCLUSION AND OUTLOOK

In summary, we have performed direct high-precision mass and double-beta decay  $Q$  value measurements of  $^{84}\text{Sr}$  using the PI-ICR technique with the JYFLTRAP double PTMS. The mass and  $Q$  values were determined with a precision approximately 30 times higher than those adopted in AME2020, aligning well with the literature. The new mass value was utilized to conduct an updated King plot analysis for transitions at 689 nm and 698 nm for  $^{84,86,87}\text{Sr}$  in relation to  $^{88}\text{Sr}$ . Our results showcase an enhanced nonlinear King plot, in good agreement with previously reported values, offering smaller uncertainties. The current contribution of the mass uncertainty to the King plot analysis enables future precision enhancements by several orders of magnitude in optical spec-

troscopy, mitigating statistical and systematic errors in both transitions. This potential advancement could lead to unparalleled sensitivity to new physics. More precise isotope shift measurements of Sr isotopes, providing stringent experimental constraints on King linearity, are highly required. Performing such a measurement with a radioactive isotope e.g.,  $^{90}\text{Sr}$ , to avoid complications due to hyperfine structure, is feasible at the IGISOL facility. In conjunction with additional measurements of isotope shifts in elements such as calcium, this will contribute to enhancing precision in atomic structure calculations and imposing constraints on new physics.

### ACKNOWLEDGMENTS

We acknowledge the staff of the Accelerator Laboratory of University of Jyväskylä (JYFL-ACCLAB) for providing sta-

ble online beam. We thank the support by the Academy of Finland under the Finnish Centre of Excellence Programme 2012-2017 (Nuclear and Accelerator Based Physics Research at JYFL) and projects No. 306980, No. 312544, No. 275389, No. 284516, No. 295207, No. 314733, No. 315179, No. 327629, No. 320062, No. 354589 and 345869. The support by the EU Horizon 2020 research and innovation program under grant No. 771036 (ERC CoG MAIDEN) is acknowledged. We express gratitude for the productive results stemming from conversations with R. de Groote and X. F. Yang.

- 
- [1] W. H. King, *Isotope Shifts in Atomic Spectra* (Plenum, New York, 1984).
- [2] V. V. Flambaum, A. J. Geddes, and A. V. Viatkina, *Phys. Rev. A* **97**, 032510 (2018).
- [3] U. Dammalapati, S. De, K. Jungmann, *et al.*, *Eur. Phys. J. D* **53**, 1 (2009).
- [4] C. Shi, F. Gebert, C. Gorges, *et al.*, *Appl. Phys. B* **123**, 2 (2017).
- [5] C. Nazé, J. G. Li, and M. Godefroid, *Phys. Rev. A* **91**, 032511 (2015).
- [6] C. Frugiuele, E. Fuchs, G. Perez, and M. Schlawfer, *Phys. Rev. D* **96**, 015011 (2017).
- [7] J. C. Berengut, D. Budker, C. Delaunay, V. V. Flambaum, C. Frugiuele, E. Fuchs, C. Grojean, R. Harnik, R. Ozeri, G. Perez, and Y. Soreq, *Phys. Rev. Lett.* **120**, 091801 (2018).
- [8] H. Miyake, N. C. Pisenti, P. K. Elgee, *et al.*, *Phys. Rev. Research* **1**, 033113 (2019).
- [9] T. Manovitz, R. Shaniv, Y. Shapira, R. Ozeri, and N. Akerman, *Phys. Rev. Lett.* **123**, 203001 (2019).
- [10] F. W. Knollmann, A. N. Patel, and S. C. Doret, *Phys. Rev. A* **100**, 022514 (2019).
- [11] I. Counts, J. Hur, D. P. L. Aude Craik, H. Jeon, C. Leung, J. C. Berengut, A. Geddes, A. Kawasaki, W. Jhe, and V. Vuletić, *Phys. Rev. Lett.* **125**, 123002 (2020).
- [12] C. Solaro, S. Meyer, K. Fisher, J. C. Berengut, E. Fuchs, and M. Drewsen, *Phys. Rev. Lett.* **125**, 123003 (2020).
- [13] D. Nesterenko, R. de Groote, T. Eronen, Z. Ge, M. Hukkanen, A. Jokinen, and A. Kankainen, *International Journal of Mass Spectrometry* **458**, 116435 (2020).
- [14] I. Counts, J. Hur, D. P. L. Aude Craik, H. Jeon, C. Leung, J. C. Berengut, A. Geddes, A. Kawasaki, W. Jhe, and V. Vuletić, *Phys. Rev. Lett.* **125**, 123002 (2020).
- [15] N.-H. Rehbahn, M. K. Rosner, H. Bekker, *et al.*, *Phys. Rev. A* **103**, L040801 (2021).
- [16] R. A. Müller, V. A. Yerokhin, A. N. Artemyev, and A. Surzhykov, *Phys. Rev. A* **104**, L020802 (2021).
- [17] J. Hur, D. P. L. A. Craik, I. Counts, *et al.*, *Phys. Rev. Lett.* **128**, 163201 (2022).
- [18] N. L. Figueroa, J. C. Berengut, V. A. Dzuba, *et al.*, *Phys. Rev. Lett.* **128**, 073001 (2022).
- [19] K. Ono, Y. Saito, T. Ishiyama, *et al.*, *Phys. Rev. X* **12**, 021003 (2022).
- [20] S. Stellmer, F. Schreck, and T. C. Killian, in *Annual Review of Cold Atoms and Molecules*, Vol. 2, edited by K. W. Madison, K. Bongs, L. D. Carr, A. M. Rey, and H. Zhai (World Scientific, Singapore, 2014) Chap. 1.
- [21] R. Rana, M. Höcker, and E. G. Myers, *Phys. Rev. A* **86**, 050502 (2012).
- [22] M. Wang, W. Huang, F. Kondev, G. Audi, and S. Naimi, *Chinese Physics C* **45**, 030003 (2021).
- [23] F. Kondev, M. Wang, W. Huang, S. Naimi, and G. Audi, *Chinese Physics C* **45**, 030001 (2021).
- [24] T. Eronen, V. S. Kolhinen, V. V. Elomaa, D. Gorelov, U. Hager, J. Hakala, A. Jokinen, A. Kankainen, P. Karvonen, S. Kopecky, I. D. Moore, H. Penttilä, S. Rahaman, S. Rinta-Antila, J. Rissanen, A. Saastamoinen, J. Szerypo, C. Weber, and J. Äystö, *European Physical Journal A* **48**, 1 (2012).
- [25] T. Eronen, A. Kankainen, and J. Äystö, *Progress in Particle and Nuclear Physics* **91**, 259 (2016).
- [26] I. D. Moore, T. Eronen, D. Gorelov, J. Hakala, A. Jokinen, A. Kankainen, V. S. Kolhinen, J. Koponen, H. Penttilä, I. Pohjalainen, M. Reponen, J. Rissanen, A. Saastamoinen, S. Rinta-Antila, V. Sonnenschein, and J. Äystö, *Nuclear Instruments and Methods in Physics Research, Section B: Beam Interactions with Materials and Atoms* **317**, 208 (2013).
- [27] P. Karvonen, I. D. Moore, T. Sonoda, T. Kessler, H. Penttilä, K. Peräjärvi, P. Ronkanen, and J. Äystö, *Nuclear Instruments and Methods in Physics Research, Section B: Beam Interactions with Materials and Atoms* **266**, 4794 (2008).
- [28] A. Nieminen, J. Huikari, A. Jokinen, J. Äystö, P. Campbell, and E. C. Cochrane, *Nuclear Instruments and Methods in Physics Research, Section A: Accelerators, Spectrometers, Detectors and Associated Equipment* **469**, 244 (2001).
- [29] G. Savard, S. Becker, G. Bollen, H. J. Kluge, R. B. Moore, T. Otto, L. Schweikhard, H. Stolzenberg, and U. Wiess, *Physics Letters A* **158**, 247 (1991).
- [30] D. A. Nesterenko, T. Eronen, A. Kankainen, L. Canete, A. Jokinen, I. D. Moore, H. Penttilä, S. Rinta-Antila, A. de Roubin, and M. Vilen, *European Physical Journal A* **54**, 0 (2018).
- [31] D. A. Nesterenko, T. Eronen, Z. Ge, A. Kankainen, and M. Vilen, *Eur. Phys. J. A* **57**, 302 (2021).
- [32] S. Eliseev, K. Blaum, M. Block, A. Dörr, C. Droese, T. Eronen, M. Goncharov, M. Höcker, J. Ketter, E. M. Ramirez,

- D. A. Nesterenko, Y. N. Novikov, and L. Schweikhard, *Applied Physics B: Lasers and Optics* **114**, 107 (2014).
- [33] S. Eliseev, K. Blaum, M. Block, C. Droese, M. Goncharov, E. Minaya Ramirez, D. A. Nesterenko, Y. N. Novikov, and L. Schweikhard, *Physical Review Letters* **110**, 82501 (2013).
- [34] A. Kramida, Yu. Ralchenko, J. Reader, and NIST ASD Team, NIST Atomic Spectra Database (ver. 5.8), [Online]. Available: <https://physics.nist.gov/asd> [2021, January 19]. National Institute of Standards and Technology, Gaithersburg, MD. (2020).
- [35] A. Kellerbauer, K. Blaum, G. Bollen, F. Herfurth, H. J. Kluge, M. Kuckein, E. Sauvan, C. Scheidenberger, and L. Schweikhard, *European Physical Journal D* **22**, 53 (2003).
- [36] C. Roux, K. Blaum, M. Block, C. Droese, S. Eliseev, M. Goncharov, F. Herfurth, E. M. Ramirez, D. A. Nesterenko, Y. N. Novikov, and L. Schweikhard, *The European Physical Journal D* **67**, 1 (2013).
- [37] R. T. Birge, *Physical Review* **40**, 207 (1932).
- [38] W. Huang, M. Wang, F. Kondev, G. Audi, and S. Naimi, *Chinese Physics C* **45**, 030002 (2021).
- [39] A. Kellerbauer, G. Audi, D. Beck, K. Blaum, G. Bollen, C. Guénaut, F. Herfurth, A. Herlert, H.-J. Kluge, D. Lunney, S. Schwarz, L. Schweikhard, C. Weber, and C. Yazidjian, *Phys. Rev. C* **76**, 045504 (2007).
- [40] E. Haettner, D. Ackermann, G. Audi, K. Blaum, M. Block, S. Eliseev, T. Fleckenstein, F. Herfurth, F. P. Heßberger, S. Hofmann, J. Ketelaer, J. Ketter, H.-J. Kluge, G. Marx, M. Mazzocco, Y. N. Novikov, W. R. Plaß, S. Rahaman, T. Rauscher, D. Rodríguez, H. Schatz, C. Scheidenberger, L. Schweikhard, B. Sun, P. G. Thirolf, G. Vorobjev, M. Wang, and C. Weber, *Phys. Rev. Lett.* **106**, 122501 (2011).
- [41] H. Booij, E. Van Hoek, H. Van Der Molen, W. Slot, and J. Blok, *Nuclear Physics A* **160**, 337 (1971).
- [42] J. Morton, W. Davies, W. Mclatchie, D. W., and J. Kitching, *Nuclear Physics A* **161**, 228 (1971).
- [43] T. Takano, R. Mizushima, and H. Katori, *Applied Physics Express* **10**, 072801 (2017).
- [44] W. H. King, *J. Opt. Soc. Am.* **53**, 638 (1963).
- [45] J. C. Berengut, D. Budker, C. Delaunay, V. V. Flambaum, C. Frugiuele, E. Fuchs, C. Grojean, R. Harnik, R. Ozeri, G. Perez, and Y. Soreq, *Phys. Rev. Lett.* **120**, 091801 (2018).
- [46] D. York, N. M. Evensen, M. L. Martinez, and J. De Basabe Delgado, *American Journal of Physics* **72**, 367 (2004).
- [47] A. D. Ludlow, M. M. Boyd, J. Ye, E. Peik, and P. O. Schmidt, *Rev. Mod. Phys.* **87**, 637 (2015).